Biochimica et Biophysica Acta 1838 (2014) 2492–2502

Contents lists available at ScienceDirect

Biochimica et Biophysica Acta

journal homepage: www.elsevier.com/locate/bbamem

Guanidino groups greatly enhance the action of antimicrobial peptidomimetics against bacterial cytoplasmic membranes

Konstantin Andreev [a,b,1], Christopher Bianchi [a,b,1], Jonas S. Laursen [c], Linda Citterio [d], Line Hein-Kristensen [e], Lone Gram [d], Ivan Kuzmenko [f], Christian A. Olsen [c], David Gidalevitz [a,b,*]

[a] Center for Molecular Study of Condensed Soft Matter (μCoSM), Pritzker Institute of Biomedical Science and Engineering, Illinois Institute of Technology, 3440 S. Dearborn St., Chicago, IL 60616, USA
[b] Department of Physics, Illinois Institute of Technology, 3440 S. Dearborn St., Chicago, IL 60616, USA
[c] Department of Chemistry, Technical University of Denmark, Kemitorvet 207, DK-2800 Kgs. Lyngby, Denmark
[d] Department of Systems Biology, Technical University of Denmark, Matematiktorvet 301, DK-2800 Kgs. Lyngby, Denmark
[e] National Food Institute, Technical University of Denmark, Søltofts Plads 221, DK-2800, Kgs Lyngby, Denmark
[f] Advanced Photon Source, Argonne National Laboratory, 9700 S. Cass Ave., Lemont, IL 60439, USA

ARTICLE INFO

Article history:
Received 21 December 2013
Received in revised form 11 May 2014
Accepted 19 May 2014
Available online 28 May 2014

Keywords:
Antimicrobial peptidomimetics
Peptide–peptoid chimeras
Guanidinium cation
Bacterial membrane
Phosphatidylglycerol
X-ray scattering

ABSTRACT

Antimicrobial peptides or their synthetic mimics are a promising class of potential new antibiotics. Herein we assess the effect of the type of cationic side chain (i.e., guanidino vs. amino groups) on the membrane perturbing mechanism of antimicrobial α-peptide–β-peptoid chimeras. Langmuir monolayers composed of 1,2-dipalmitoyl-*sn*-glycero-3-phosphatidylglycerol (DPPG) were used to model cytoplasmic membranes of both Gram-positive and Gram-negative bacteria, while lipopolysaccharide Kdo2-lipid A monolayers were mimicking the outer membrane of Gram-negative species. We report the results of the measurements using an array of techniques, including high-resolution synchrotron surface X-ray scattering, epifluorescence microscopy, and *in vitro* antimicrobial activity to study the molecular mechanisms of peptidomimetic interaction with bacterial membranes. We found guanidino group-containing chimeras to exhibit greater disruptive activity on DPPG monolayers than the amino group-containing analogues. However, this effect was not observed for lipopolysaccharide monolayers where the difference was negligible. Furthermore, the addition of the nitrobenzoxadiazole fluorophore did not reduce the insertion activity of these antimicrobials into both model membrane systems examined, which may be useful for future cellular localization studies.

1. Introduction

Antimicrobial peptides (AMPs) are ubiquitous in nature; present in virtually all organisms they serve as endogenous antibiotics through the innate immune response [1,2]. Members of this class of compounds have been studied extensively due to their potential as promising alternative antibiotics to treat disease caused by the growing number of resistant pathogenic microbes [1–4]. It is generally believed that AMPs exert their direct killing of invading pathogens by selectively interacting with the negatively charged bacterial surfaces over the globally neutral (zwitterionic) eukaryotic cell membranes. The mechanism by which the membranes are permeated is not completely understood, and several models have been proposed based on studies conducted with various peptidic structures [1]. Moreover, recent studies have shown that some of these chemotypes are endowed with additional intracellular modes of action such as interference with cell wall biosynthesis or immunomodulatory effects [5–9]. These findings complicate the understanding of this class of compounds even further and have called for the use of a perhaps more appropriate class designation, host-defense peptides (HDPs) [3].

Despite their diversity in amino acid sequence, lipophilicity and secondary structure [10], most HDPs share common features including positive net charge and generally amphipathic nature, separating hydrophilic and hydrophobic residues to the opposite faces of the molecule [11–13]. Typically, positive net charge of naturally occurring peptides is contributed by the guanidino groups of the arginine (Arg) [14,15] and/or amino groups of the lysine (Lys) residues [16–18]. Both Arg and Lys side chains are generally thought to promote the initial long range electrostatic attractive forces that guide antimicrobials towards the negatively charged bacterial membranes [19]. However, guanidino groups have higher acid dissociation constant (pK_a) due to efficient resonance stabilization of the charged protonated state together with efficient solvation in water, which makes them stronger bases and, thus, better suited for stable electrostatic interactions with the negatively charged phosphodiester and phosphomonoester groups

* Corresponding author Department of Physics, Illinois Institute of Technology, 3440 S. Dearborn St., Chicago, IL 60616, USA. Tel.: +1 312 567 3534; fax: +1 312 567 8856.
E-mail address: gidalevitz@iit.edu (D. Gidalevitz).
[1] These authors contributed equally to the work.

http://dx.doi.org/10.1016/j.bbamem.2014.05.022
0005-2736/

of phospholipids [20–24]. Examples of naturally occurring AMPs containing arginine rather than lysine residues include several members of the cathelicidin family, such as indolicidin and tritrpticin [25,26]. Also, in peptides having high content of both arginine and lysine residues such as the defensins, these residues are not randomly distributed within their sequence and their ordering implies a significance greater than just a net positive charge [27]. Muhle and Tam [28] found that Arg-to-Lys substitution in a cyclic disulfide-stabilized peptide decreased activity against Gram-negative bacteria. Nakase *et al.* demonstrated improved membrane permeability of antimicrobial peptide (RLA) with lysine substituted by arginine [29]. Other studies have shown that for lactoferricin B and bactenecin 5, which have no hemolytic activity, the replacement of arginine for lysine reduced antibacterial activity [30]. So, the incorporation of guanidino groups into the peptide side chains may have its appeal in drug design [31–33].

However, there are concerns related to the use of α-peptides in a clinical setting due to their high cost of manufacturing [34] and inherent susceptibility to proteases [35], which has led to numerous studies aimed at mimicry of peptides using non-natural compounds. Thus, a variety of classes such as β-peptides [36–38], oligoureas [39], arylamides [40,41], *N*-substituted oligoglycines (peptoids) [42–44], cyclic D,L-α-peptides [45–47], hybrid peptidomimetics [33,48–50], and polymers [51–53] have been designed to mimic the function of AMPs.

α-Peptide–β-peptoid chimeras represent a distinct class of peptidomimetics with backbone composed of alternating peptide and β-peptoid residues [33,50,54–56]. In the present study we elucidate the role of the cation type on the antimicrobial properties of this type of synthetic AMP mimics using two α-peptide–β-peptoid chimeras ($K\beta N_{spe}$ and $R\beta N_{spe}$), which differ from each other solely in the identity of cationic functionality [amine (lysine) vs. guanidino group (homoarginine)]. In addition, because fluorophore-labeled analogues of AMPs, which retain antimicrobial activity, constitute powerful tools for studying mechanisms of action and cellular localization, we also prepared and evaluated nitrobenzoxadiazole (NBD)-labeled oligomers NBD-$K\beta N_{spe}$ and NBD-$R\beta N_{spe}$ (Fig. 1A).

Regardless of whether the primary mode of action is of a membrane-disrupting nature or entails perturbation of intracellular targets, the initial interaction between antimicrobial and bacteria involves the cell surface. A fundamental understanding of these lipid–antimicrobial interactions is therefore important for the future design of improved antibiotics for potential clinical use. Since cell membranes have a complex structure and are currently not applicable for highly sensitive surface X-ray scattering methods, the model systems are generally employed to undertake detailed mechanistic studies of membrane-associated processes [57–61]. Previously, the membrane-destabilizing effects of the α-peptide–β-peptoid chimeras have only been investigated in model liposomes prepared from phosphatidylcholine (PC), a phospholipid found predominantly in eukaryotic cells [55]. However, PC-containing systems do not adequately represent bacterial envelope, and furthermore, these compounds have not been investigated using sensitive X-ray methods before.

In order to model the outer surface of Gram-positive and Gram-negative bacteria we have employed insertion assay experiments on two separate Langmuir monolayers composed of 1,2-dipalmitoyl-sn-glycero-3-phosphatidylglycerol (DPPG) and truncated lipopolysaccharide (LPS) Kdo2-Lipid A, respectively (Fig. 1B). The reason behind this choice of lipids is that Kdo-2 lipid A constitutes the hydrophobic core of outer LPS envelope in most Gram-negative bacteria, while PGs are predominant anionic phospholipid species within cytoplasmic membranes of both Gram-negative and Gram-positive strains. This approach has been successfully used in conjunction with liquid surface X-ray scattering to study bacterial membrane lysis by human antimicrobial peptide LL-37 [60], protegrin-1 [57,62], gramicidin [63] and SMAP-29 [61] antimicrobial peptides as well as by peptide mimics [44,49,59,64].

2. Experimental section

2.1. Monolayer construction

Both DPPG and Kdo2-Lipid A were purchased from Avanti Polar Lipids (Alabaster, AL) and were used without further purification. To form the monolayer systems both DPPG and Kdo2-Lipid A were first dissolved in chloroform–methanol (65:25) at a concentration of 0.2 mg/mL. Using a microliter syringe (Hamilton) the solutions were

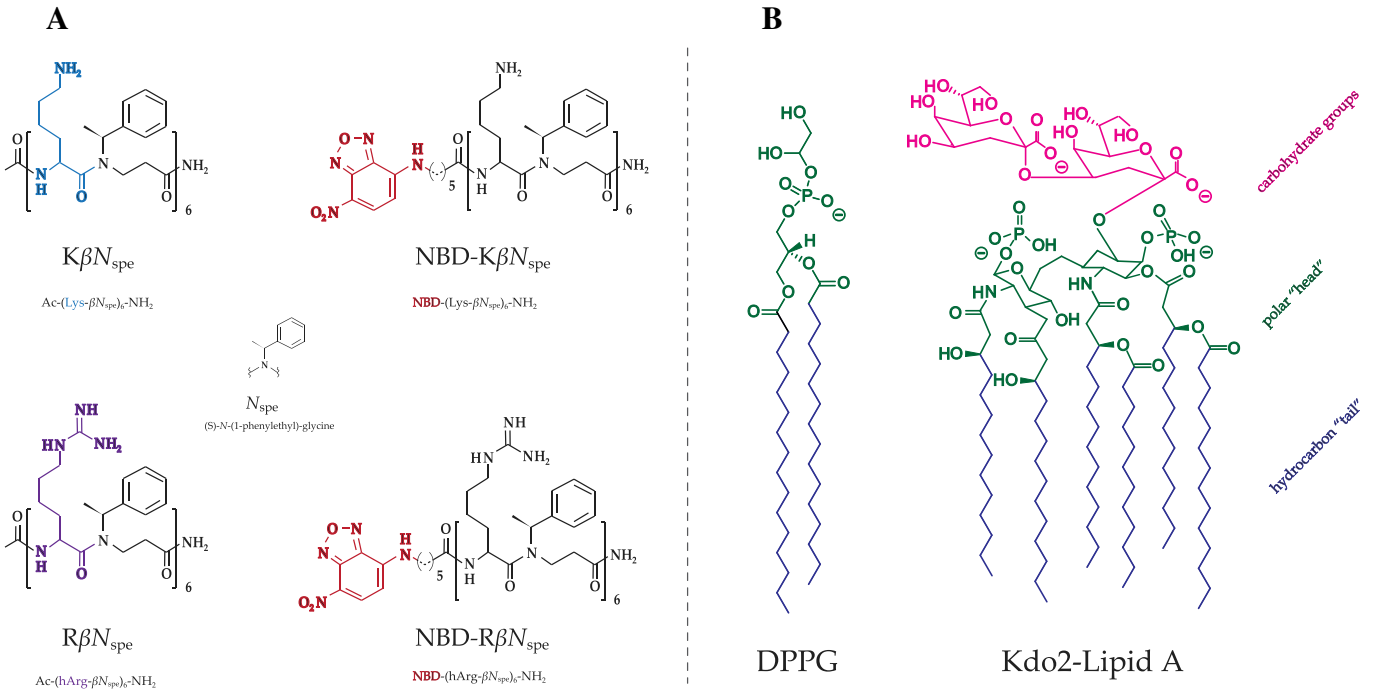

Fig. 1. Molecular structures of the tested chimeras (A) and lipids used for modeling bacterial cell membranes (B).

then spread on the surface of a Dulbecco's phosphate buffered saline (DPBS) (Invitrogen, Carlsbad, Ca) void of calcium and magnesium ions contained in a single barrier Langmuir trough. Over 15 min the organic solvents evaporated to form a self-assembled monolayer. The monolayer was then compressed to a biologically relevant packing density of 30 $mN \times m^{-1}$, which was monitored by a Wilhelmy plate. This surface pressure and a temperature of 22 ± 0.5 °C were maintained throughout the experiment. As a result, if changes in the surface pressure occur, the barrier will have to move in order to maintain the set surface pressure. Such change in barrier position then allows for change in area/lipid molecule or area/LPS molecule ΔA to be calculated. Once the monolayer was compressed the chamber containing the Langmuir trough was sealed and purged with helium to lower the oxygen levels in the chamber, which minimizes background X-ray scattering during the X-ray experiments [58,65].

2.2. X-ray reflectivity (XR)

XR gives the information about electron density gradient along the plane perpendicular to the surface of a monolayer as well as about the film thickness [66–68]. A slab-model, also known as a box model, was used to analyze XR data. This model is based on the Parratt recursive method [69] that describes the interface as a stack of slabs with distinct electron densities (ρ), and thicknesses (l) [70–74]. The final fit was achieved by minimizing the χ^2 value while ensuring that parameters obtained were physically relevant. The software used to fit experimental XR data was RFit2000 [75–77]. In addition to model-dependent approach, model-independent stochastic fitting, where the electron-density profile is parameterized using cubic B-splines was also performed [78].

2.3. Grazing-incidence X-ray diffraction (GIXD)

Grazing incidence X-ray diffraction measurements were performed to monitor the effect of compound insertion on the molecular packing of the lipid monolayers [79]. Lipid films spread at the air–water interface may be described by a large number of two-dimensional crystalline domains of ordered hydrocarbon chains randomly oriented around the surface normal [80]. In a GIXD experiment, the momentum transfer has a horizontal and vertical component, Q_{xy} and Q_z [81]. The Q_{xy} positions of the observed Bragg peaks yield the repeat distances, $d_{hk} = 2\pi / q_{hk}$ for the 2D lattice, from which specific parameters (a, b, γ) of the crystal system can be extracted. From the full-width half-maximum (FWHM) values of Bragg peaks, the in-plane coherence length, L_{xy} was calculated using the Scherrer formula, $L_{xy} = 0.9 \times 2\pi$ / FWHM. The intensity distribution along the Bragg rod was measured at Bragg peak positions to evaluate the tilt of acyl chains.

All X-ray measurements were done at sector 9-ID at the Advanced Photon Source (APS) of Argonne National Labs (Chicago IL) with an X-ray wavelength of 0.9202 Å. After XR and GIXD were performed on a given monolayer system α-peptide–β-peptoid hybrids were introduced into the system using a bent needle syringe (Hamilton). The needle is placed underneath the barrier and the compounds were injected underneath the monolayer to mimic the approach of the compound from the extracellular fluid to the outer leaflet of the membrane. After injection both XR and GIXD measurements were taken for comparison.

2.4. Real-time epifluorescence microscopy (EFM) imaging

Morphological changes of DPPG films were studied on a microscopic level before and after the introduction of α-peptide–β-peptoid chimeras according to protocols previously described [64,82]. Briefly, the Langmuir trough setup and procedures used in the formation of the lipid monolayers were essentially the same, except that a 0.1 mol% of lipid-linked Texas Red dye [TR-DHPE (Molecular Probes, Eugene, OR)] was premixed with stock DPPG solution. A heated glass-plate was placed over the trough to reduce contamination and evaporation of the subphase during the experiment.

2.5. Chemical synthesis

2.5.1. Fmoc-Lys(Dde)-βNspe-OH (**8**)

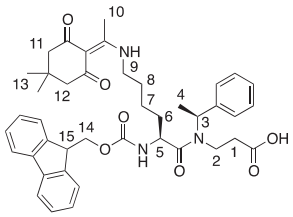

Fmoc-Lys-β*N*spe-OH (**7**) (1.61 g, 2.96 mmol) and *i*Pr_2NEt (1.4 mL, 8.0 mmol) were dissolved in DMF (30 mL), and added acetyl dimedone (913 mg, 5.0 mmol). After stirring for 18 h, the solvent was evaporated in vacuo and the crude product redissolved in EtOAc (100 mL). The solution was washed with 1 M HCl (aq) (2 × 100 mL) and water (2 × 100 mL), dried (Na_2SO_4), filtered, and evaporated in vacuo to give 1.22 g (82%) of the desired product as a white solid. ^{1}H NMR (300 MHz, CD_3OD), δ 1.48 (m, 2H, H-7), 1.66/1.56* (2 × d, 3H, J = 7.0 Hz, H-4), 1.68–1.82 (broad m, 4H, H-6, H-8), 2.17/2.51 (3 × m, 2H, H-1), 2.27*/2.28/2.51*/2.52 (4 × m, 6H, H-11, H-12) 3.19/3.38 (2 × m, 2H, H-2), 3.48 (m, 5H, H-9, H-10), 4.17 (m, 1H, H-15), 4.27–4.43 (broad m, 2H, H-14), 4.52*/4.81 (2 × m, 2H, H-5) 5.42/5.81* (2 × q, 1H, J = 7.0 Hz, H-3), 7.23–7.41 (broad m, 9H, Ph, Fmoc ArH), 7.66 (m, 2H, Fmoc ArH) 7.79 (d, 2H, J = 7.5 Hz, Fmoc Ar). $[\alpha]_{589.2}$: −46° (c = 1.0, 293 K, $CHCl_3$). UPLC-MS gradient A, t_R = 2.20 min (>95), MS: (m/z) $[M + H]^+$ calcd. for $C_{32}H_{38}N_3O_5^+$: 708.9, found: 708.6. HRMS: (m/z) $[M + H]^+$ calcd. for $C_{32}H_{38}N_3O_5^+$: 708.3643, found: 708.3649 (ΔM = 0.8 ppm).

2.5.2. Solid-phase synthesis of **9**

Fmoc-protected Rink amide resin (590 mg, 0.25 mmol) was treated with piperidine–DMF (1:4, 5 mL, 2 × 20 min), and washed with DMF, MeOH, and CH_2Cl_2 (3 × 5 mL). Oligomerization was performed with a mixture of Fmoc-Lys(Dde)-β*N*spe-OH (**8**) (750 mg, 1.1 mmol, 4.5 equiv), HBTU (417 mg, 1.1 mmol, 4.5 equiv), and *i*Pr_2NEt (0.38 mL, 2.2 mmol, 9 equiv) in DMF (5 mL), which were preincubated for 10 min before being added to the Rink amide resin and shaken for 18 h. After each coupling the resin was washed with MeOH, DMF and CH_2Cl_2 (3 × 5 mL). Fmoc deprotection was achieved with piperidine–DMF (1:4, 5 mL, 2 × 20 min) followed by DBU–piperidine–DMF (2:2:96, 5 mL, 2 × 20 min), after each deprotection step the resin was washed using the same procedure as above. This three-step coupling/deprotection sequence was performed 6 times to give the resin-bound oligomer.

2.5.3. Ac-(Lys-βNspe)$_6$-NH$_2$ (KβN_{spe})

The terminal amino groups of (**9**) (100 mg, 0.024 mmol) were capped with a mixture of Ac_2O–*i*Pr_2NEt–DMF (1:2:3, 2 mL, 2 h) and the resin was washed with DMF, MeOH, and CH_2Cl_2 (3 × 2 mL). The side chains were deprotected using 2% hydrazine in DMF (2 × 2 mL, 45 min). The crude product was cleaved from the support with 50% TFA–CH_2Cl_2 (2 mL, 2 × 1 h). The TFA was co-evaporated with toluene (3 × 30 mL), toluene–CH_2Cl_2 (3 × 30 mL), and CH_2Cl_2 (3 × 3 mL). The residue was purified by preparative RP-HPLC (gradient C) and fractions were lyophilized to give KβN_{spe} as white fluffy material [12.3 mg, 15% (90% per step)]. HPLC gradient D, t_R = 10.47 (>95%). HRMS: m/z $[M + 3H]^{3+}$ calcd for $C_{104}H_{158}N_{19}O_{13}^{3+}$: 627.07567, found: 627.07553 (ΔM: 0.22 ppm) [50].

2.5.4. Ac-(hArg-βNspe)$_6$-NH$_2$ (RβN$_{spe}$)

The terminal amino group of (**9**) (75 mg, 0.024 mmol) was capped with a mixture of Ac_2O–*i*Pr_2NEt–DMF (1:2:3, 2 mL, 2 h) and the resin was washed with DMF, MeOH, and CH_2Cl_2 (3 × 2 mL). The side chains were deprotected using 2% hydrazine in DMF (2 × 2 mL, 2 × 45 min), and washed as above. Boc-protected guanidino groups were introduced by addition of a mixture of *N*,*N*′-bis(*tert*-butoxycarbonyl)-1H-pyrazole-1-carboxamidine (**11**) (285 mg, 0.92 mmol) and *i*Pr_2NEt (0.32 mL, 1.84 mmol) in DMF for 18 h, followed by the above washing procedure. The crude guanidinium-containing product was simultaneously deprotected and cleaved from the support with TFA–CH_2Cl_2 (1:1, 2 mL, 2 × 1 h). The TFA was co-evaporated with toluene (3 × 30 mL), toluene–CH_2Cl_2 (3 × 30 mL) and CH_2Cl_2 (3 × 30 mL). The residue was purified by preparative RP-HPLC (gradient C) and fractions were lyophilized to give RβN$_{spe}$ as white fluffy material [12.9 mg, 20% (90% per step)]. HPLC gradient D, t_R = 10.39 (>95%). HRMS: *m*/*z* $[M + 3H]^{3+}$ calcd for $C_{110}H_{170}N_{31}O_{13}^{3+}$: 711.1193, found: 711.1190 (ΔM: 0.35 ppm) [50].

2.5.5. NBD-(Lys-βNspe)$_6$-NH$_2$ (NBD-KβN$_{spe}$)

A Rink amide resin-bound oligomer with Boc protected lysine side chains (150 mg, 0.039 mmol) was prepared as described for **9** using the Fmoc-Lys(Boc)-β*N*spe-OH [83] building block. The N-terminal was then functionalized with a mixture of *N*-NBD-6-aminohexanoic acid (73 mg, 0.25 mmol), *i*Pr_2NEt (87 μL, 0.5 mmol), and PyBOP (156 mg, 0.3 mmol) in DMF (2 mL). After shaking for 18 h, the resin was washed with DMF, MeOH, and CH_2Cl_2 (3 × 2 mL), and the compound was cleaved from the support using TFA–CH_2Cl_2 (1:1, 2 mL, 2 × 1 h). Trifluoroacetic acid was co-evaporated with toluene (3 × 30 mL), toluene–CH_2Cl_2 (3 × 30 mL), and CH_2Cl_2 (3 × 3 mL), and the residue was purified by preparative RP-HPLC (gradient C). Lyophilization of the fractions containing the title compound furnished a yellow fluffy material [12.5 mg, 15% (88% per step)]. HPLC gradient D, t_R = 10.29 (>95%). HRMS: *m*/*z* $[M + 3H]^{3+}$ calcd. for $C_{114}H_{168}N_{23}O_{16}^{3+}$: 705.4352, found: 705.4361 (ΔM: 1.3 ppm), and *m*/*z* $[M + 4H]^{4+}$ calcd. for $C_{114}H_{169}N_{23}O_{16}^{4+}$: 529.3252, found: 529.3261 (ΔM: 1.7 ppm).

2.5.6. NBD-(hArg-βNspe)$_6$-NH$_2$ (NBD-RβN$_{spe}$)

Crude NBD-(Lys-β*N*spe)$_6$-NH_2 (NBD-KβN$_{spe}$) (30 mg, 0.014 mmol) and *i*Pr_2NEt (29 μL, 0.16 mmol) were dissolved in DMF (2 mL), followed by addition of *N*,*N*′-bis(*tert*-butoxycarbonyl)-1H-pyrazole-1-carboxamidine (40 mg, 0.13 mmol). After stirring for 3 h, the solvent was evaporated in vacuo, and excess reagent removed by vacuum silica gel chromatography [2 × 6 cm, CH_2Cl_2–MeOH 0.5% gradient 0 → 10% (containing 1% concentrated aqueous NH_3)]. The product was then deprotected with TFA–CH_2Cl_2 (1:1, 2 mL, 2 × 1 h) and TFA was removed by co-evaporation with toluene (3 × 30 mL), toluene–CH_2Cl_2 (3 × 30 mL), and CH_2Cl_2 (3 × 3 mL). The compound was purified by preparative RP-HPLC (gradient C) to give NBD-RβN$_{spe}$ as a yellow fluffy material (5 mg, 15%). HPLC gradient D, t_R = 11.05 (>95%). HRMS: *m*/*z* $[M + 4H]^{4+}$ calcd. for $C_{120}H_{181}N_{35}O_{16}^{4+}$: 592.5609, found: 592.5603 (ΔM: 1 ppm).

Details of synthetic procedures, characterization data, as well as ^1H and ^{13}C NMR spectra for all new compounds are presented in Supporting Information.

2.6. Bacterial strains and culture conditions

Activity experiments (Minimum Inhibitory Concentration and Minimum Bactericidal Concentration) were carried out with eight bacterial species representing common laboratory strains and clinical strains derived from both food-borne and nosocomial infections. The strains also represented Gram-positive and Gram-negative species. Stock cultures were stored at −80 °C in 4% (w/v) glycerol, 0.5% (w/v) glucose, 2% (w/v) skimmed milk powder, and 3% (w/v) tryptone soy powder. All experiments were carried out with bacteria incubated for one night (approximately 18 h) at 37 °C. Experiments were performed in cation-adjusted Mueller Hinton II broth [MHB (Becton Dickinson 212322)] adjusted to pH 7.4. MHB was supplemented with 1.25% defibrinated horseblood (Statens Seruminstitut REF23699) to ensure growth of *Bacillus cereus* and *Streptococcus pyogenes*. Brain Heart Infusion (CM1135) with 1.5% agar (VWR 20768.292) as gelling agent was used throughout for colony plating.

2.7. Antimicrobial activity assay

MIC and MBC were determined using the micro-dilution method according to guidelines of the Clinical and Laboratory Standards Institute (CLSI). Two-fold serial dilutions of the peptidomimetic hybrids were prepared from 1024 μg/mL stock solutions in Milli-Q water to give a final range of 512–0.5 μg/mL in the wells. Colonies grown on BHI agar for approximately 18 h were suspended in 0.9% saline to give a turbidity of 0.13 at OD_{546} (approximately 1 × 10^8 CFU/mL), and then diluted in MHB pH 7.4 to a final concentration of approx. 5 × 10^5 CFU/mL in each well. Polypropylene plates (Nunc 442587) were used to minimize peptide binding, and the incubation time was 18–20 h at 37 °C. MIC values, i.e., the lowest concentration of the peptide analogue at which no visible growth was observed, were determined in duplicate. Platings were done from all wells where no visible growth was observed and the lowest concentration of peptide analogue at which no growth occurred on BHI plates was denoted the MBC, the Minimal Bactericidal Concentration Activity expressed in μg/mL.

3. Results

3.1. Synthesis

The syntheses of chimeras were achieved by preparation of dimeric building blocks followed by oligomerization on solid support using variations of previously described methods [50,83,84]. In order to enable an on-resin functionalization of the lysine ε-amino groups we installed an orthogonal 1-(4,4-dimethyl-2,6-dioxacyclohexylidene) ethyl (Dde) group [85,86] on the lysine side chain functionality to give building block **8** (Scheme 1).

For the standard Fmoc solid-phase peptide synthesis (SPPS) oligomerization, a Chem-Matrix® resin was chosen due to its excellent swelling properties in a variety of solvents. After six rounds of coupling/deprotection (**9**), the N-terminal was acetylated and the Dde group was removed to give **10**, which upon cleavage afforded KβN$_{spe}$ (Scheme 2). Functionalization of the free amines in **10** by guanidinylation [87], followed by simultaneous deprotection and cleavage furnished RβN$_{spe}$. Unfortunately, introduction of the fluorophore proved incompatible with our new protecting group strategy, most likely due to sensitivity towards hydrazine during the Dde deprotection step. For the syntheses of labeled analogues NBD-KβN$_{spe}$ and NBD-KβN$_{spe}$, a different strategy involving guanidinylation in solution was therefore adopted as shown in Supplementary Scheme S1 and Scheme S2.

3.2. Antimicrobial activities

MIC and MBC assays clearly demonstrated greater bacteriostatic and bactericidal properties of RβN$_{spe}$ against all eight examined strains. The favorable effect of guanidinium cation was highly pronounced for Gram-positive bacteria (fourfold difference in MICs and MBCs) and moderate for Gram-negative ones. The toxicity of KβN$_{spe}$ and RβN$_{spe}$ against human erythrocytes was previously determined using hemolytic assay and considered to be negligible [33].

In our recent studies, fluorescein-labeled versions of α-peptide–β-peptoid chimeras have been prepared to investigate their potential as cell-penetrating peptides [54,55], and subsequent antimicrobial testing of these showed a severe decrease in potency when introducing the fluorescein label [33]. Herein, we therefore tested the NBD-labeled

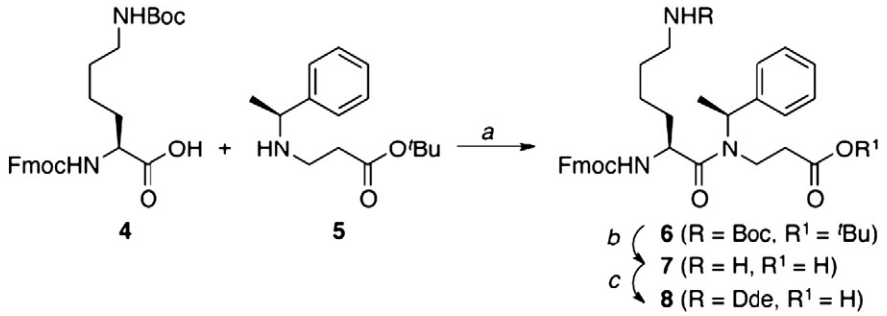

Scheme 1. Synthesis of dimeric building block **8**. Reagents and conditions: (*a*) Fmoc-Lys(Boc)-OH (1.7 equiv), HBTU (1.7 equiv), *i*Pr2NEt (4 equiv), DMF, 18 h. (*b*) TFA–CH_2Cl_2 (4:6), 2 h. (*c*) Acetyl dimedone (1.7 equiv), *i*Pr2NEt (2.7 equiv), DMF, 18 h.

chimeras for their antimicrobial activity against a selection of pathogens to determine if the novel fluorescent-labeled antimicrobial could inhibit bacterial growth. Interestingly, MIC and MBC values of NBD-tagged amino-containing chimera were found to be lower against all Gram-positive and Gram-negative strains tested (except *Vibrio vulnificus*). However for guanidino-containing antimicrobials the trend is opposite. Since the effect of NBD-fluorophore can be either attenuating or enhancing but within acceptable range of the parent compounds, we decided to include fluorescently tagged chimeras in the model study along with KβN_{spe} and RβN_{spe}.

3.3. Epifluorescence microscopy

EFM images of the DPPG monolayer at 30 mN × m^{-1} display an array of branched dark domains of condensed phase ~25–50 μm in diameter separated from each other by brightly colored "fluid" (disordered) areas. Fig. 2 shows the dynamics of surface morphology changes in lipid film after injection of KβN_{spe} and RβN_{spe} into the subphase. Both compounds caused a decrease in the size of condensed-phase domains starting from the 4th min and followed by their complete elimination with transition of the majority of the film to a liquid-disordered phase after 15–20 min. Structurally ordered regions in this case might be either fully destroyed or reduced in size to become smaller than the microscope resolution (<1 μm). This points out to a crystallinity-disruptive behavior of the studied α-peptide–β-peptoid chimeras against DPPG monolayers regardless of the identity of the cations they contain, at least on micrometer scale.

3.4. Specular X-ray reflectivity

Fig. 3 shows electron density profiles along the surface normal extracted from reflectivity data by model-independent stochastic fitting. The graphs are combined in such a way as to allow visual comparison of amino- and guanidino-containing chimeras. For the lipid monomolecular films, the electron density is zero at the air–water interface, then rises sharply through the hydrocarbon tail region, and comes to a plateau reaching its maximum values for the head groups (at a distance of ~20–25 Å from the air side of the film) before slightly decaying to the subphase electron density. In addition, model-dependent analyses were performed on XR data. Pure DPPG monolayers were modeled as two slabs, with the first slab corresponding to the phospholipid acyl chains, and the second reperesenting the lipid head groups. XR analysis yielded the thickness of the slab related to acyl chains to be 16.5 Å with an electron density of 0.312 $e^-/Å^3$. The thickness of the slab used to model the head groups was found to be 8.3 Å with an electron density of 0.477 $e^-/Å^3$. Two-slab model-dependent fitting of Kdo-2 Lipid A data yielded 12.0 Å long upper hydrocarbon chain region with electron density of 0.31 $e^-/Å^3$. The second slab corresponding to the complex of head moieties and the outer layer of carbohydrate 3-deoxy-D-mannooctulosonic acid known as Kdo has the thickness of 12.8 Å and an electron density of 0.485 $e^-/Å^3$. Insertion of antimicrobials into the membrane mimic results in extra electrons per lipid molecule in each slab and is calculated using formula (1).

$$N_{extra}e^-_{slab} = l_{slab} \times \rho_{slab} \times \left(A_{lipid} + \Delta A_{lipid}\right) - N_{initial}e^-_{slab} \quad (1)$$

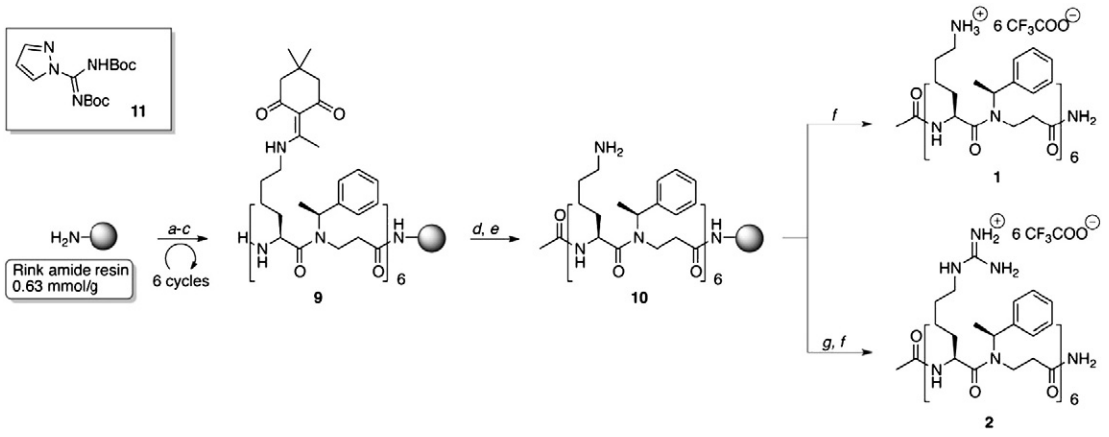

Scheme 2. Solid supported oligomerization of building block **8**. Reagents and conditions: (*a*) **8** (4.5 equiv), HBTU (4.5 equiv), *i*Pr2NEt (9 equiv), DMF, 18 h. (*b*) Piperidine–DMF (1:4), 2 × 10 min. (*c*) DBU–piperidine–DMF (2:2:96), 20 min. (*d*) Ac2O–*i*Pr2NEt–DMF (1:2:3), 2 h. (*e*) Hydrazine–DMF (2:98), 2 × 45 min. (*f*) 50% TFA–CH_2Cl_2, 2 × 1 h. (*g*) *N*,*N*′-Bis(*tert*butoxycarbonyl)-1H-pyrazole-1-carboxamidine (**11**, 36 equiv), *i*Pr2NEt (72 equiv), DMF, 18 h. HBTU = *O*-(Benzotriazol-1-yl)-*N*,*N*,*N*′,*N*′-tetramethyluronium hexafluorophosphate.

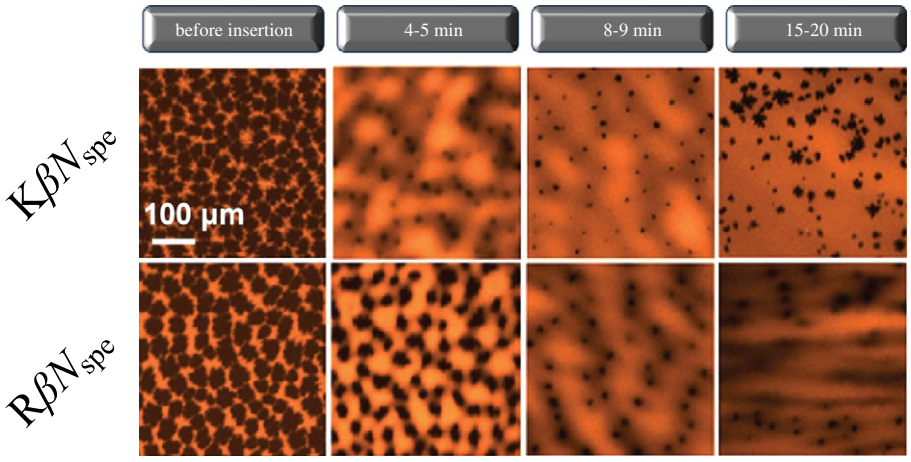

Fig. 2. Epifluorescence images of DPPG monolayers after injection of N_{spe}K (A) and N_{spe}R (B) at concentrations corresponding to 20% of their MIC values observed against *Staphylococcus aureus* respectively. Lipid-linked Texas Red-DHPE fluorescence probe (1 mol%) was added to the phospholipid solutions for EFM experiments. Because of steric hindrance, the dye is located in the liquid-disordered phase, rendering it bright whereas the liquid-ordered phase remains dark.

Here, l_{slab} and ρ_{slab} are thickness and electron density of the slab, respectively; $A_{lipid} + \Delta A_{lipid}$ is the area per lipid molecule upon insertion and $N_{initial}\, e^-_{slab}$ minus the number of electrons in the slab in the original untreated monolayer.

Preliminary information about the mode of antimicrobial interaction with membrane mimics can be obtained directly from the electron density profiles (Fig. 3A). KβN_{spe} and RβN_{spe} displayed a drastic difference in their mode of action against DPPG monolayers. Following injection of KβN_{spe} the first minimum of reflectivity curve shifted from $q_z \approx 0.24$ Å^{-1} to a higher q_z value with the peak of electron density moved towards the air–water interface. This indicates a decrease in thickness of the film as a result of its insertion. However, RβN_{spe} instead of thinning DPPG monolayer, led to appearance of two minima on the reflectivity profile at $q_z \approx 0.21$ Å^{-1} and 0.35 Å^{-1} and a notable bump of the electron density curve within the range of 20–40 Å away from the air–water interface. This might be due to an additional layer of distinct electron density higher than the electron density of subphase present underneath the head group region. These data are corroborated by the model-dependent analysis and are summarized in Supplementary Table S1. Injection of KβN_{spe} into DPPG resulted in an experimental XR curve, which was again best fit with two layers. However, an additional box was required to fit XR data upon introduction of RβN_{spe}. The lower increase in area per lipid molecule observed upon insertion of RβN_{spe} as compared with KβN_{spe} could possibly be explained by partial dimerization or aggregation of guanidino-containing chimera on the outer surface of lipid monolayer. According to the number of extra electrons contributed by incorporated antimicrobials, both KβN_{spe} and RβN_{spe} readily insert into the polar moieties of DPPG and Kdo-2 Lipid A resulting in reduced electron density of bottom slab, but they are both unable to penetrate deeply into overlying hydrophobic core of lipid monolayers. The more substantial decrease in electron density of the DPPG head group region, along with three times more additional electrons present upon introduction of RβN_{spe} points to a higher Gram-positive membrane disruptive potential of guanidino-containing compound versus its amino-containing counterpart. The same trend was observed for the NBD-tagged chimeras. Here compound NBD-RβN_{spe} permeated the entire depth of DPPG film including hydrophobic acyl chains, whereas NBD-KβN_{spe} was found only in the hydrophilic outer shell of the lipid monolayer. Furthermore, the introduction of NBD-RβN_{spe} led to a greater contribution of additional electrons in toto, as well as to a four-fold larger increase in area per single DPPG molecule (ΔA_{lipid}) indicating a favorable effect of arginine residues on the antimicrobial insertion.

In contrast to DPPG, the reflectivity curves of Kdo-2 Lipid A monolayer after introduction of KβN_{spe} and RβN_{spe} look nearly identical (Fig. 3B). For model-dependent analysis two boxes were sufficient to fit experimental XR data and revealed very similar mechanism of action utilized by guanidino- and amino-containing chimeras against Gram-negative bacteria LPS. This consistency in mode of action between KβN_{spe} and RβN_{spe}, as well as between NBD-KβN_{spe} and NBD-RβN_{spe} was confirmed by similar changes in thickness of respective slabs within Kdo-2 Lipid A monolayer and by similar number of contributed extra electrons. The area increase per lipid molecule in both pairs of compounds was also about the same.

Additionally, the effect of NBD-fluorophore was investigated by comparing KβN_{spe} and RβN_{spe} to their NBD-tagged fluorescent analogues NBD-KβN_{spe} and NBD-RβN_{spe} respectively. According to the results of XR analysis, functionalization of α-peptide–β-peptoid chimeras by NBD does not reduce their capability to interact with model bacterial membranes. Moreover, fluorophore-carrying chimeras have provided even greater contribution of additional electrons to the lipid head-groups. This implies a higher number of chimeras to be inserted into the lipid films.

3.5. Grazing-incidence X-ray diffraction

GIXD data for DPPG monolayer before and after injection of antimicrobials are presented in Fig. 4. The corresponding values of unit cell dimensions, *d*-spacings and sizes of crystallized domains are presented in Table 2. At the surface pressure of 30 mN × m^{-1} pure DPPG yields two distinct Bragg peaks at $Q_{xy} = 1.39$ Å^{-1} and $Q_{xy} = 1.47$ Å^{-1} corresponding to *d*-spacings of 4.51 and 4.26 Å, respectively. This indicates the presence of ordered structure with the centered rectangular packing ($a \neq b$, $\gamma = 90°$) having unit cell dimensions $a = 5.32$ Å and $b = 8.54$ Å and an area of 45.5 Å^2 per single DPPG molecule. For Kdo2-Lipid A, on the other hand, no Bragg peak was observed. This means that there were no diffractable 2D crystalline regions within the monolayer, which does not allow a detailed analysis of the surface morphology. According to GIXD data, RβN_{spe} and NBD-RβN_{spe} fully destroy the lateral crystallinity of DPPG monolayers evidenced by complete disappearance of Bragg peaks. Conversely, both KβN_{spe} and NBD-KβN_{spe}, instead of disordering, caused structural rearrangement of the crystal lattice from a centered rectangular crystal packing to a hexagonal ($a = b$, $\gamma = 120°$) resulting in appearance of a single Bragg peak. The coherence length was also reduced, which might explain the disappearance of ordered regions upon introduction of KβN_{spe} observed by EFM. Furthermore, NBD-KβN_{spe} was shown to decrease the size of crystallized domains as well as the order of their crystallinity to a greater extent than its non-labeled counterpart, even though the main parameters of crystal lattice didn't change much. This supports the hypothesis that

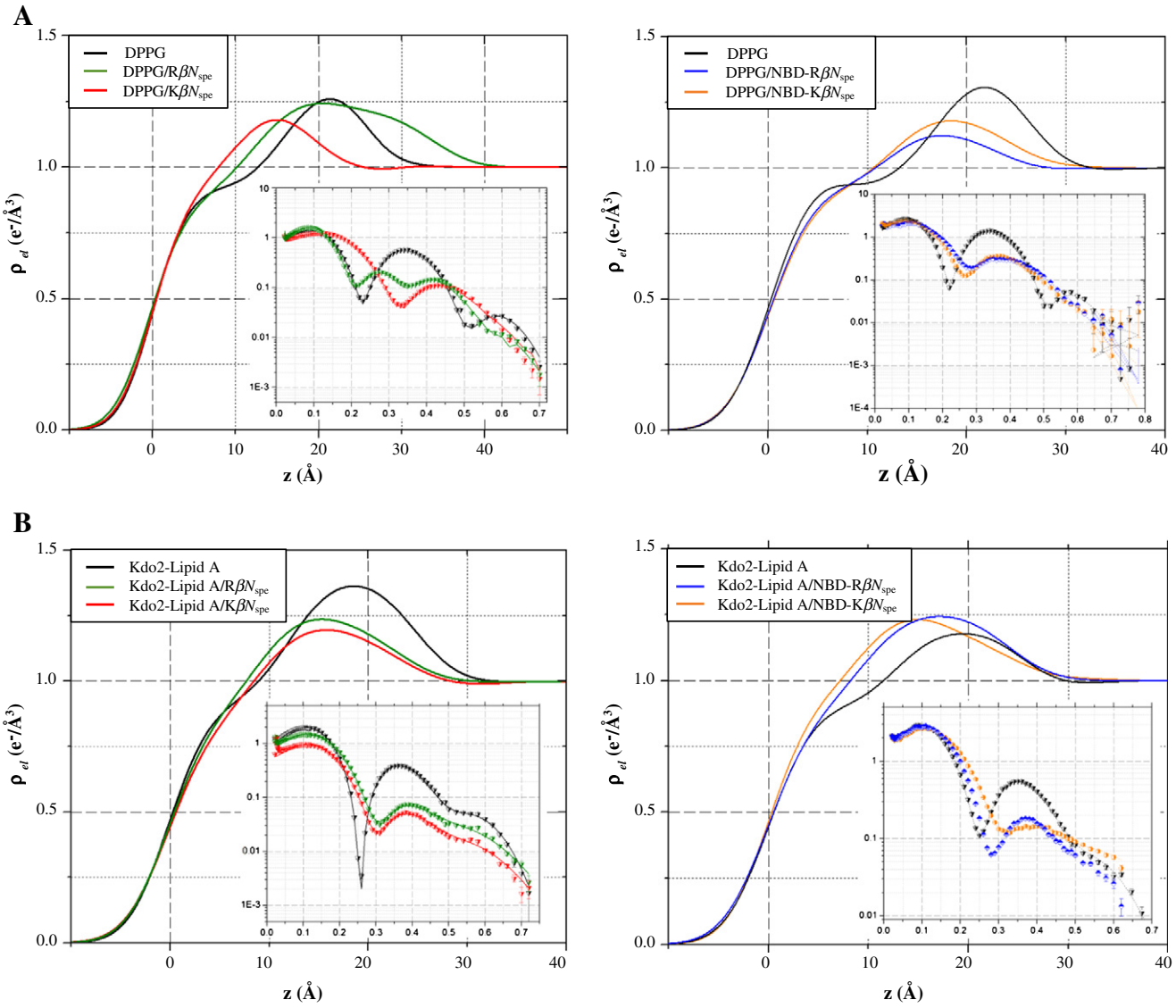

Fig. 3. Electron density profiles and corresponding Fresnel-divided reflectivity curves against the scattering vector (q) in the z direction (q_z) for DPPG (A) and Kdo2-Lipid A (B) monolayers at 30 mN × m^{-1}. Electron density profiles were normalized to the electron density of the subphase buffer. On the XR graphs, the scatter plots are experimental values and solid lines are the best fits of the models to the experimental data. Fresnel reflectivity is the reflectivity from ideal smooth surface.

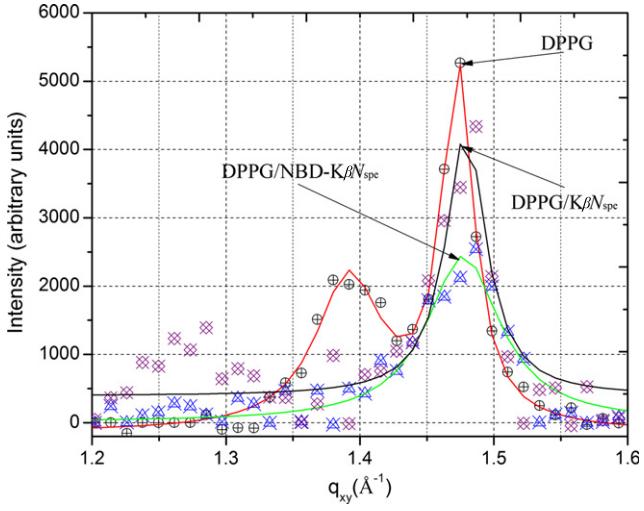

Fig. 4. Bragg peaks plot of scattering vector Q_{xy} as a function of intensity.

labeling of antimicrobials with NBD may enhance their disruptive potential against phosphatidylglycerol-containing membranes without drastically changing the primary mechanism of action. (See Table 1.)

4. Discussion

Overall, our data provide solid mechanistic evidence of higher membrane activity against Gram-positive strains displayed by guanidino-containing α-peptide–β-peptoid chimeras as compared to their amino-substituted counterparts. Guanidino groups were shown to considerably improve the capability of antimicrobial peptidomimetics to compromise the integrity of DPPG monolayers mimicking the external leaflet of Gram-positive bacteria cell membranes. These XR data are in excellent agreement with the previously published results [33,56]. Same trend however was not observed for lipopolysaccharide (Kdo-2 Lipid A) monolayers, which model the outer membrane surface of Gram-negative species. The higher antimicrobial activity of guanidino-containing chimeras in vitro in this case might be due to that fact that Gram-negative bacteria have both outer and cytoplasmic membranes. When passing through the outer (LPS-rich) shell both amino- and guanidino-containing chimeras follow similar self-promoted uptake

Table 1
Antimicrobial and hemolytic activities of α-peptide–β-peptoid chimeras.

Activity		Target strain	MIC, MBC and HC_{10} measurements for selected pathogens (μg×mL^{-1})[a]			
			KβN$_{spe}$	NBD-KβN$_{spe}$	RβN$_{spe}$	NBD-RβN$_{spe}$
MIC						
	Gram-negative	*E. coli*[b]	64	64	8	64
		E. coli[c]	128	32	16	64
		K. pneumoniae[d]	256	128	32	128
		V. vulnificus[e]	16	16–32	8	64
	Gram-positive	*S. aureus*[f]	256	64	32	128
		S. epidermidis[g]	16–64	8–16	4	16
		S. pyogenes[h]	16–32	8–16	4–8	16–32
		B. cereus[i]	64–128	16–32	4–8	16
MBC						
	Gram-negative	*E. coli*[b]	64	64	8	64
		E. coli[c]	128	64	16	64
		K. pneumoniae[d]	256	128	64	128
		V. vulnificus[e]	32	64	8	64
	Gram-positive	*S. aureus*[f]	>256	128	32	128
		S. epidermidis[g]	32–64	8–16	4–8	16–32
		S. pyogenes[h]	16–32	8–16	4–8	16–32
		B. cereus[i]	128	16–32	4–8	16
HC_{10} hRBCs [33]			>500	ND	>500	ND

[a] MIC = Minimum Inhibitory Concentration: lowest concentration without visible growth; MBC = Minimum Bactericidal Concentration: lowest concentration where cell growth could not be detected by plating. The values are based on two individual experiments conducted in duplicate. HC_{10} = concentration that causes 10% hemolysis, hRBCs = human red blood cells, ND = not determined.
[b] *Escherichia coli* ATCC 25922.
[c] *Escherichia coli* AAS-EC-009 [Extended Spectrum Beta-Lactamase (ESBL)-producing clinical sample isolated from a Danish patient in 2007].
[d] *K. pneumoniae* = *Klebsiella pneumoniae* ATCC 13883.
[e] *V. vulnificus* = *Vibrio vulnificus* cmcP6 (clinical isolate provided by Joon Haeng Rhee) [88].
[f] *S. aureus* = *Staphylococcus aureus* 8325-4.
[g] *S. epidermidis* = *Staphylococcus epidermidis* RP62A.
[h] *S. pyogenes* = *Streptococcus pyogenes* GAS-1 [clinical isolate kindly provided by the Statens Serum Institute, Copenhagen, Denmark].
[i] *B. cereus* = *Bacillus cereus* ATCC 11778.

mechanism, by which bivalent cations are displaced causing a destabilization of the LPS core and the entry into the periplasmic space. However, in order to kill bacteria, it might be not enough just to permeate/damage its outer membrane; the cytoplasmic membrane needs to be affected as well. Because of the high content of phosphatidylglycerol lipid species within the inner membrane guanidino-containing chimeras have better capability to disrupt it that leads to their stronger bactericidal properties. A full explanation of this finding, however, would require extensive experiments beyond the scope of this work. A schematic cartoon illustrating the proposed mechanism of membrane interaction utilized by tested antimicrobials is represented in Fig. 5.

As both types of cations are fully protonated at physiological pH we hypothesize that the ability of the guanidino group to form a more stable bidentate electrostatic interaction with negatively charged phosphodiester moieties affects the DPPG lipids to a greater extent than the more structurally rigid Kdo-2 Lipid A. These findings thus provide fundamental insights that should be useful in the future design of optimized synthetic peptidomimetics with selective antibiotic effects.

Finally, addition of the NBD fluorophore did not significantly reduce the insertion activity of the tested chimeras into model membranes that also correlate with their retained antimicrobial potency in vitro, especially for NBD-KβN_{spe}. Moreover, the NBD-labeled chimeras demonstrated even greater ability to destroy both DPPG and Kdo-2 Lipid A monolayers, than their non-tagged analogues. It is assumed that this is a result of increased lipophilicity of modified molecules due to incorporation of the hydrophobic benzofurazan ring of NBD. The resulting amphiphilic properties may reduce the energy penalties associated with penetration of antimicrobials into hydrophobic core and, thus, favor the disruption of membrane structure. The use of fluorescently tagged AMP mimics might facilitate future cellular localization studies aimed at the elucidation of the mechanism of action of oligomeric AMPs in general.

Table 2
Structural parameters of crystal monolayer lattice.

Sample	Peak position (Å^{-1})	*d*-Spacing (Å)	Unit cell parameters	L_{xy}[a] (Å)	Area unit cell (Å^2)
DPPG	Q_{xy1} = 1.39, Q_{xy2} = 1.47	d_n = 4.51 d_{o2} = 4.26[b]	a = 5.32 Å b = 8.54 Å y = 90° θ = 27°	L_{11} = 93 L_{02} = 196	44.51
DPPG/KβN_{spe}	1.48	4.25	a = 6.93 Å y = 120° θ = 0°	156	41.62
DPPG/NBD-KβN$_{spe}$	1.48	4.25	a = 6.94 Å y = 120° θ = 0°	85	41.69
DPPG/RβN$_{spe}$ and DPPG/NBD-RβN$_{spe}$ displayed no visible GIXD peaks					

[a] Table Coherence length (L_{xy}) = the average distance in the direction of the reciprocal lattice vector Q_{xy} over which the domain is ordered.
[b] "11" and "02" are used to denote (*hk*) vectors in reciprocal space.

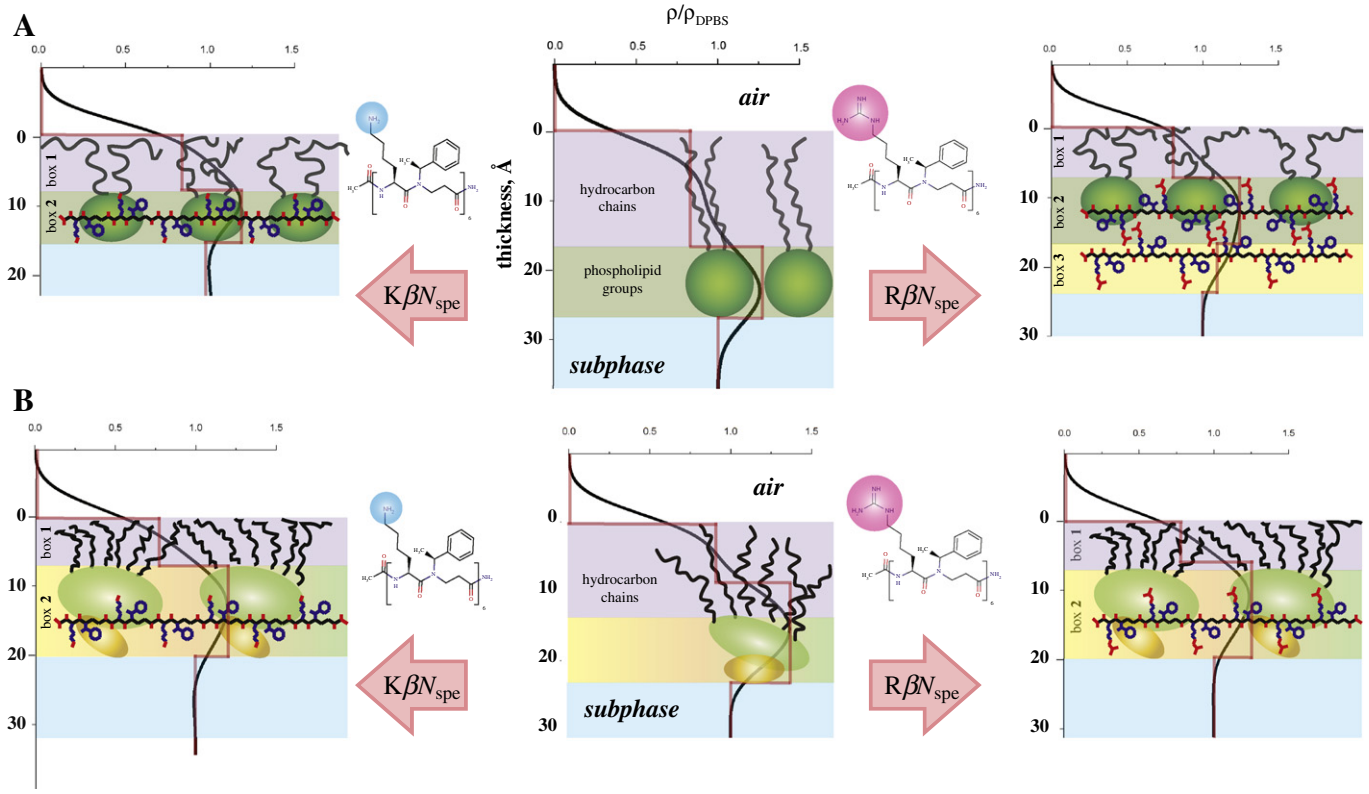

Fig. 5. Cartoon schematic of possible interactions of KβN_{spe}K and RβN_{spe}R with (A) DPPG and (B) Kdo-2 Lipid A monolayers at 30 mN×m^{-1}. Chimeras carrying amino groups are solely located in the polar head-moieties of DPPG accompanied with considerable thinning of the entire monolayer, whereas their guanidino-substituted analogues form an extra layer on the surface of lipid film resulting in more compact distribution of inserted molecules within the model membrane. Unlike DPPG, the insertion mechanisms of KβN_{spe} and RβN_{spe} into Kdo-2 Lipid A model look nearly identical.

Acknowledgements

We thank Dr. Andrey Ivankin for assistance with synchrotron X-ray scattering experiments, Ms. Anne Hector and Dr. Charlotte H. Gotfredsen for assistance with NMR spectroscopy, and Ms. Tina Gustafsson for technical assistance with UPLC-MS and HRMS. The National Center for Antimicrobials & Infection Control, Statens Serum Institut, Denmark is acknowledged for providing the Danish clinical sample of ESBL-producing *Escherichia coli* and the *S. pyogenes* strain.

This work was supported by funds from NIH (R01 AI073892, D.G.), DARPA (W911NF-09-1-378, D.G.), the Danish Research Council for Technology and Production (09-065902 and 09-066098), the Danish Independent Research Council | Natural Sciences (Steno Grant no. 10-080907, C.A.O.), and the Technical University of Denmark. Use of the APS was supported by DOE under contract no. W-31-109-Eng-38. C.A.O. is also supported by the Lundbeck Foundation.

Appendix A. Supplementary data

Supplementary data to this article can be found online at http://dx.doi.org/10.1016/j.bbamem.2014.05.022.

References

[1] M. Zasloff, Antimicrobial peptides of multicellular organisms, Nature 415 (2002) 389–395.
[2] R.E.W. Hancock, H.G. Sahl, Antimicrobial and host-defense peptides as new anti-infective therapeutic strategies, Nat. Biotechnol. 24 (2006) 1551–1557.
[3] A.T.Y. Yeung, S.L. Gellatly, R.E.W. Hancock, Multifunctional cationic host defence peptides and their clinical applications, Cell. Mol. Life Sci. 68 (2011) 2161–2176.
[4] J.L. Fox, Antimicrobial peptides stage a comeback, Nat. Biotechnol. 31 (2013) 379–382.
[5] E. Breukink, I. Wiedemann, C. van Kraaij, O.P. Kuipers, H.G. Sahl, B. de Kruijff, Use of the cell wall precursor lipid II by a pore-forming peptide antibiotic, Science 286 (1999) 2361–2364.
[6] T. Schneider, T. Kruse, R. Wimmer, I. Wiedemann, V. Sass, U. Pag, A. Jansen, A.K. Nielsen, P.H. Mygind, D.S. Ravents, S. Neve, B. Ravn, A.M.J.J. Bonvin, L. De Maria, A. S. Andersen, L.K. Gammelgaard, H.G. Sahl, H.H. Kristensen, Plectasin, a fungal defensin, targets the bacterial cell wall precursor lipid II, Science 328 (2010) 1168–1172.
[7] S. Sandgren, A. Wittrup, F. Cheng, M. Jonsson, E. Eklund, S. Busch, M. Belting, The human antimicrobial peptide LL-37 transfers extracellular DNA plasmid to the nuclear compartment of mammalian cells via lipid rafts and proteoglycan-dependent endocytosis, J. Biol. Chem. 279 (2004) 17951–17956.
[8] K.A. Brogden, Antimicrobial peptides: pore formers or metabolic inhibitors in bacteria? Nat. Rev. Microbiol. 3 (2005) 238–250.
[9] M.G. Scott, E. Dullaghan, N. Mookherjee, N. Glavas, M. Waldbrook, A. Thompson, A.K. Wang, K. Lee, S. Doria, P. Hamill, J.J. Yu, Y.X. Li, O. Donini, M.M. Guarna, B.B. Finlay, J.R. North, R.E.W. Hancock, An anti-infective peptide that selectively modulates the innate immune response, Nat. Biotechnol. 25 (2007) 465–472.
[10] C.D. Fjell, J.A. Hiss, R.E.W. Hancock, G. Schneider, Designing antimicrobial peptides: form follows function, Nat. Rev. Drug Discov. 11 (2012) 37–51.
[11] Z. Oren, Y. Shai, Mode of action of linear amphipathic alpha-helical antimicrobial peptides, Biopolymers 47 (1998) 451–463.
[12] R.E. Hancock, Host defence (cationic) peptides: what is their future clinical potential? Drugs 57 (1999) 469–473.
[13] Z. Jiang, A.I. Vasil, J.D. Hale, R.E. Hancock, M.L. Vasil, R.S. Hodges, Effects of net charge and the number of positively charged residues on the biological activity of amphipathic alpha-helical cationic antimicrobial peptides, Biopolymers 90 (2008) 369–383.
[14] D.A. Steinberg, M.A. Hurst, C.A. Fujii, A.H.C. Kung, J.F. Ho, F.C. Cheng, D.J. Loury, J.C. Fiddes, Protegrin-1: a broad-spectrum, rapidly microbicidal peptide with in vivo activity, Antimicrob. Agents Chemother. 41 (1997) 1738–1742.
[15] M.H. Wu, R.E.W. Hancock, Interaction of the cyclic antimicrobial cationic peptide bactenecin with the outer and cytoplasmic membrane, J. Biol. Chem. 274 (1999) 29–35.
[16] M. Zasloff, Magainins, a class of antimicrobial peptides from *Xenopus* skin: isolation, characterization of two active forms, and partial cDNA sequence of a precursor, Proc. Natl. Acad. Sci. U. S. A. 84 (1987) 5449–5453.
[17] Y. Ge, D.L. MacDonald, K.J. Holroyd, C. Thornsberry, H. Wexler, M. Zasloff, In vitro antibacterial properties of pexiganan, an analog of magainin, Antimicrob. Agents Chemother. 43 (1999) 782–788.
[18] D. Savoia, R. Guerrini, E. Marzola, S. Salvadori, Synthesis and antimicrobial activity of dermaseptin S1 analogues, Bioorg. Med. Chem. 16 (2008) 8205–8209.

[19] T. Hessa, H. Kim, K. Bihlmaier, C. Lundin, J. Boekel, H. Andersson, I. Nilsson, S.H. White, G. von Heijne, Recognition of transmembrane helices by the endoplasmic reticulum translocon, Nature 433 (2005) 377–381.
[20] Y.C. Su, T. Doherty, A.J. Waring, P. Puchala, M. Hong, Roles of arginine and lysine residues in the translocation of a cell-penetrating peptide from C-13, P-31, and F-19 solid-state NMR, Biochemistry 48 (2009) 4587–4595.
[21] M. Hong, Y.C. Su, Structure and dynamics of cationic membrane peptides and proteins: insights from solid-state NMR, Protein Sci. 20 (2011) 641–655.
[22] P.A. Gale, Special issue: anion coordination chemistry II — preface, Coord. Chem. Rev. 250 (2006) 2917.
[23] J. Mavri, H.J. Vogel, Ion pair formation of phosphorylated amino acids and lysine and arginine side chains: a theoretical study, Proteins 24 (1996) 495–501.
[24] A.S. Woods, S. Ferre, Amazing stability of the arginine-phosphate electrostatic interaction, J. Proteome Res. 4 (2005) 1397–1402.
[25] L.T. Nguyen, L. de Boer, S.A. Zaat, H.J. Vogel, Investigating the cationic side chains of the antimicrobial peptide tritrpticin: hydrogen bonding properties govern its membrane-disruptive activities, Biochim. Biophys. Acta 1808 (2011) 2297–2303.
[26] S.T. Yang, S.Y. Shin, C.W. Lee, Y.C. Kim, K.S. Hahm, J.I. Kim, Selective cytotoxicity following Arg-to-Lys substitution in tritrpticin adopting a unique amphipathic turn structure, FEBS Lett. 540 (2003) 229–233.
[27] R.A. Llenado, C.S. Weeks, M.J. Cocco, A.J. Ouellette, Electropositive charge in alpha-defensin bactericidal activity: functional effects of Lys-for-Arg substitutions vary with the peptide primary structure, Infect. Immun. 77 (2009) 5035–5043.
[28] S.A. Muhle, J.P. Tam, Design of Gram-negative selective antimicrobial peptides, Biochemistry 40 (2001) 5777–5785.
[29] I. Nakase, S. Okumura, S. Katayama, H. Hirose, S. Pujals, H. Yamaguchi, S. Arakawa, S. Shimizu, S. Futaki, Transformation of an antimicrobial peptide into a plasma membrane-permeable, mitochondria-targeted peptide via the substitution of lysine with arginine, Chem. Commun. (Camb.) 48 (2012) 11097–11099.
[30] Y. Tokunaga, T. Niidome, T. Hatakeyama, H. Aoyagi, Antibacterial activity of bactenecin 5 fragments and their interaction with phospholipid membranes, J. Pept. Sci. 7 (2001) 297–304.
[31] F. Saczewski, L. Balewski, Biological activities of guanidine compounds, Expert Opin. Ther. patents 19 (2009) 1417–1448.
[32] B. Findlay, P. Szelemej, G.G. Zhanel, F. Schweizer, Guanidylation and tail effects in cationic antimicrobial lipopeptoids, PLoS ONE 7 (2012) e41141.
[33] C.A. Olsen, H.L. Ziegler, H.M. Nielsen, N. Frimodt-Moller, J.W. Jaroszewski, H. Franzyk, Antimicrobial, hemolytic, and cytotoxic activities of beta-peptoid-peptide hybrid oligomers: improved properties compared to natural AMPs, Chembiochem 11 (2010) 1356–1360.
[34] A. Giuliani, G. Pirri, S.F. Nicoletto, Antimicrobial peptides: an overview of a promising class of therapeutics, Cent. Eur. J. Biol. 2 (2007) 1–33.
[35] S.M. Miller, R.J. Simon, S. Ng, R.N. Zuckermann, J.M. Kerr, W.H. Moos, Proteolytic studies of homologous peptide and N-substituted glycine peptoid oligomers, Bioorg. Med. Chem. Lett. 4 (1994) 2657–2662.
[36] Y. Hamuro, J.P. Schneider, W.F. DeGrado, De novo design of antibacterial β-peptides, J. Am. Chem. Soc. 121 (1999) 12200–12201.
[37] E.A. Porter, X. Wang, H.S. Lee, B. Weisblum, S.H. Gellman, Non-haemolytic beta-amino-acid oligomers, Nature 404 (2000) 565.
[38] P.I. Arvidsson, J. Frackenpohl, N.S. Ryder, B. Liechty, F. Petersen, H. Zimmermann, G.P. Camenisch, R. Woessner, D. Seebach, On the antimicrobial and hemolytic activities of amphiphilic beta-peptides, Chembiochem 2 (2001) 771–773.
[39] A. Violette, S. Fournel, K. Lamour, O. Chaloin, B. Frisch, J.P. Briand, H. Monteil, G. Guichard, Mimicking helical antibacterial peptides with nonpeptidic folding oligomers, Chem. Biol. 13 (2006) 531–538.
[40] G.N. Tew, D. Liu, B. Chen, R.J. Doerksen, J. Kaplan, P.J. Carroll, M.L. Klein, W.F. DeGrado, De novo design of biomimetic antimicrobial polymers, Proc. Natl. Acad. Sci. U. S. A. 99 (2002) 5110–5114.
[41] S. Choi, A. Isaacs, D. Clements, D. Liu, H. Kim, R.W. Scott, J.D. Winkler, W.F. DeGrado, De novo design and in vivo activity of conformationally restrained antimicrobial arylamide foldamers, Proc. Natl. Acad. Sci. U. S. A. 106 (2009) 6968–6973.
[42] B. Goodson, A. Ehrhardt, S. Ng, J. Nuss, K. Johnson, M. Giedlin, R. Yamamoto, W.H. Moos, A. Krebber, M. Ladner, M.B. Giacona, C. Vitt, J. Winter, Characterization of novel antimicrobial peptoids, Antimicrob. Agents Chemother. 43 (1999) 1429–1434.
[43] J.A. Patch, A.E. Barron, Helical peptoid mimics of magainin-2 amide, J. Am. Chem. Soc. 125 (2003) 12092–12093.
[44] N.P. Chongsiriwatana, J.A. Patch, A.M. Czyzewski, M.T. Dohm, A. Ivankin, D. Gidalevitz, R.N. Zuckermann, A.E. Barron, Peptoids that mimic the structure, function, and mechanism of helical antimicrobial peptides, Proc. Natl. Acad. Sci. U. S. A. 105 (2008) 2794–2799.
[45] S. Fernandez-Lopez, H.S. Kim, E.C. Choi, M. Delgado, J.R. Granja, A. Khasanov, K. Kraehenbuehl, G. Long, D.A. Weinberger, K.M. Wilcoxen, M.R. Ghadiri, Antibacterial agents based on the cyclic D,L-alpha-peptide architecture, Nature 412 (2001) 452–455.
[46] V. Dartois, J. Sanchez-Quesada, E. Cabezas, E. Chi, C. Dubbelde, C. Dunn, J. Granja, C. Gritzen, D. Weinberger, M.R. Ghadiri, T.R. Parr Jr., Systemic antibacterial activity of novel synthetic cyclic peptides, Antimicrob. Agents Chemother. 49 (2005) 3302–3310.
[47] L. Motiei, S. Rahimipour, D.A. Thayer, C.H. Wong, M.R. Ghadiri, Antibacterial cyclic D, L-alpha-glycopeptides, Chem. Commun. (Camb.) (2009) 3693–3695.
[48] I.S. Radzishevsky, S. Rotem, D. Bourdetsky, S. Navon-Venezia, Y. Carmeli, A. Mor, Improved antimicrobial peptides based on acyl-lysine oligomers, Nat. Biotechnol. 25 (2007) 657–659.
[49] F. Zaknoon, H. Sarig, S. Rotem, L. Livne, A. Ivankin, D. Gidalevitz, A. Mor, Antibacterial properties and mode of action of a short acyl-lysyl oligomer, Antimicrob. Agents Chemother. 53 (2009) 3422–3429.
[50] C.A. Olsen, G. Bonke, L. Vedel, A. Adsersen, M. Witt, H. Franzyk, J.W. Jaroszewski, Alpha-peptide/beta-peptoid chimeras, Org. Lett. 9 (2007) 1549–1552.
[51] K. Kuroda, W.F. DeGrado, Amphiphilic polymethacrylate derivatives as antimicrobial agents, J. Am. Chem. Soc. 127 (2005) 4128–4129.
[52] B.P. Mowery, S.E. Lee, D.A. Kissounko, R.F. Epand, R.M. Epand, B. Weisblum, S.S. Stahl, S.H. Gellman, Mimicry of antimicrobial host-defense peptides by random copolymers, J. Am. Chem. Soc. 129 (2007) 15474–15476.
[53] F. Nederberg, Y. Zhang, J.P.K. Tan, K.J. Xu, H.Y. Wang, C. Yang, S.J. Gao, X.D. Guo, K. Fukushima, L.J. Li, J.L. Hedrick, Y.Y. Yang, Biodegradable nanostructures with selective lysis of microbial membranes, Nat. Chem. 3 (2011) 409–414.
[54] L. Vedel, G. Bonke, C. Foged, H. Ziegler, H. Franzyk, J.W. Jaroszewski, C.A. Olsen, Antiplasmodial and prehemolytic activities of alpha-peptide-beta-peptoid chimeras, ChemBioChem 8 (2007) 1781–1784.
[55] C. Foged, H. Franzyk, S. Bahrami, S. Frokjaer, J.W. Jaroszewski, H.M. Nielsen, C.A. Olsen, Cellular uptake and membrane-destabilizing properties of alpha-peptide/beta-peptoid chimeras: lessons for the design of new cell-penetrating peptides, Biochim. Biophys. Acta Biomembr. 1778 (2008) 2487–2495.
[56] L. Hein-Kristensen, K.M. Knapp, H. Franzyk, L. Gram, Bacterial membrane activity of alpha-peptide/beta-peptoid chimeras: influence of amino acid composition and chain length on the activity against different bacterial strains, BMC Microbiol. 11 (2011) 144.
[57] D. Gidalevitz, Y. Ishitsuka, A.S. Muresan, O. Konovalov, A.J. Waring, R.I. Lehrer, K.Y. Lee, Interaction of antimicrobial peptide protegrin with biomembranes, Proc. Natl. Acad. Sci. U. S. A. 100 (2003) 6302–6307.
[58] A. Ivankin, B. Apellaniz, D. Gidalevitz, J.L. Nieva, Mechanism of membrane perturbation by the HIV-1 gp41 membrane-proximal external region and its modulation by cholesterol, Biochim. Biophys. Acta 1818 (2012) 2521–2528.
[59] A. Ivankin, L. Livne, A. Mor, G.A. Caputo, W.F. Degrado, M. Meron, B. Lin, D. Gidalevitz, Role of the conformational rigidity in the design of biomimetic antimicrobial compounds, Angew. Chem. Int. Ed. Engl. 49 (2010) 8462–8465.
[60] F. Neville, M. Cahuzac, O. Konovalov, Y. Ishitsuka, K.Y. Lee, I. Kuzmenko, G.M. Kale, D. Gidalevitz, Lipid headgroup discrimination by antimicrobial peptide LL-37: insight into mechanism of action, Biophys. J. 90 (2006) 1275–1287.
[61] F. Neville, A. Ivankin, O. Konovalov, D. Gidalevitz, A comparative study on the interactions of SMAP-29 with lipid monolayers, Biochim. Biophys. Acta 1798 (2010) 851–860.
[62] F. Neville, Y. Ishitsuka, C.S. Hodges, O. Konovalov, A.J. Waring, R. Lehrer, K.Y. Lee, D. Gidalevitz, Protegrin interaction with lipid monolayers: grazing incidence X-ray diffraction and X-ray reflectivity study, Soft Matter 4 (2008) 1665–1674.
[63] C. Whitehouse, D. Gidalevitz, M. Cahuzac, R.E. Koeppe Ii, A. Nelson, Interaction of gramicidin derivatives with phospholipid monolayers, Langmuir 20 (2004) 9291–9298.
[64] H. Sarig, L. Livne, V. Held-Kuznetsov, F. Zaknoon, A. Ivankin, D. Gidalevitz, A. Mor, A miniature mimic of host defense peptides with systemic antibacterial efficacy, FASEB J. 24 (2010) 1904–1913.
[65] A. Ivankin, I. Kuzmenko, D. Gidalevitz, Cholesterol–phospholipid interactions: new insights from surface X-ray scattering data, Phys. Rev. Lett. 104 (2010) 108101.
[66] M. Losche, Surface-sensitive X-ray and neutron scattering characterization of planar lipid model membranes and lipid/peptide interactions, Curr. Top. Membr. 52 (2002) 117 (-+).
[67] M. Schalke, M. Losche, Structural models of lipid surface monolayers from X-ray and neutron reflectivity measurements, Adv. Colloid Interf. Sci. 88 (2000) 243–274.
[68] T.R. Jensen, K. Balashev, T. Bjornholm, K. Kjaer, Novel methods for studying lipids and lipases and their mutual interaction at interfaces. Part II. Surface sensitive synchrotron X-ray scattering, Biochimie 83 (2001) 399–408.
[69] L.G. Parratt, Surface studies of solids by total reflection of X-rays, Phys. Rev. 95 (1954) 359.
[70] K. Kjaer, Some simple ideas on X-ray reflection and grazing-incidence diffraction from thin surfactant films, Physica B 198 (1994) 100–109.
[71] K. Kjaer, J. Alsnielsen, C.A. Helm, P. Tippmankrayer, H. Mohwald, Synchrotron X-ray-diffraction and reflection studies of arachidic acid monolayers at the air–water-interface, J. Phys. Chem. 93 (1989) 3200–3206.
[72] J.S. Pedersen, I.W. Hamley, Analysis of neutron and X-ray reflectivity data by constrained least-squares methods, Physica B 198 (1994) 16–23.
[73] H. Mohwald, Phospholipid and phospholipid–protein monolayers at the air/water interface, Annu. Rev. Phys. Chem. 41 (1990) 441–476.
[74] M. Thoma, M. Schwendler, H. Baltes, C.A. Helm, T. Pfohl, H. Riegler, H. Mohwald, Ellipsometry and X-ray reflectivity studies on monolayers of phosphatidylethanolamine and phosphatidylcholine in contact with n-dodecane, n-hexadecane, and bicyclohexyl, Langmuir 12 (1996) 1722–1728.
[75] O.V. Konovalov, L.A. Feigin, B.M. Shchedrin, Statistical evaluation of the accuracy of structure parameter determination from X-ray and neutron reflectivity data, Kristallografiya 41 (1996) 640–643.
[76] O.V. Konovalov, L.A. Feigin, B.M. Shchedrin, Allowance for apparatus distortions in modeling the structure of Langmuir–Blodgett films from reflectivity data, Kristallografiya 41 (1996) 629–634.
[77] I.I. Samoilenko, O.V. Konovalov, L.A. Feigin, B.M. Shchedrin, L.G. Yanusova, Processing of experimental reflectivity data within the REFLAN software package, Crystallogr. Rep. 44 (1999) 310–318.
[78] S.M. Danauskas, D. Li, M. Meron, B. Lin, K.Y.C. Lee, Stochastic fitting of specular X-ray reflectivity data using StochFit, J. Appl. Crystallogr. 41 (2008) 1187–1193.
[79] T.R. Jensen, K. Kjaer, Structural properties and interactions of thin films at the air–liquid interface explored by synchrotron X-ray scattering, Stud. Interf. Sci. 11 (2001) 205–254.
[80] J. Als-Nielsen, D. Jacquemain, K. Kjaer, F. Leveiller, M. Lahav, L. Leiserowitz, Principles and applications of grazing-incidence X-ray and neutron-scattering from ordered molecular monolayers at the air–water-interface, Phys. Rep. 246 (1994) 252–313.
[81] D. Jacquemain, S.G. Wolf, F. Leveiller, M. Deutsch, K. Kjaer, J. Als-Nielsen, M. Lahav, L. Leiserowitz, Two-dimensional crystallography of amphiphilic molecules at the air–water interface, Angew. Chem. Int. Ed. Engl. 31 (1992) 130–152.

[82] H. Brockman, Lipid monolayers: why use half a membrane to characterize protein–membrane interactions? Curr. Opin. Struct. Biol. 9 (1999) 438–443.
[83] G. Bonke, L. Vedel, M. Witt, J.W. Jaroszewski, C.A. Olsen, H. Franzyk, Dimeric building blocks for solid-phase synthesis of alpha-peptide–beta-peptoid chimeras, Synthesis-Stuttgart (2008) 2381–2390.
[84] J.S. Laursen, J. Engel-Andreasen, P. Fristrup, P. Harris, C.A. Olsen, Cis–trans amide bond rotamers in beta-peptoids and peptoids: evaluation of stereoelectronic effects in backbone and side chains, J. Am. Chem. Soc. 135 (2013) 2835–2844.
[85] J.J. Diaz-Mochon, L. Bialy, M. Bradley, Full orthogonality between Dde and Fmoc: the direct synthesis of PNA–peptide conjugates, Org. Lett. 6 (2004) 1127–1129.
[86] W.C. Chan, B.W. Bycroft, D.J. Evans, P.D. White, A novel 4-aminobenzyl ester-based carboxy-protecting group for synthesis of atypical peptides by Fmoc-Bu(T) solid-phase chemistry, J. Chem. Soc. Chem. Commun. (1995) 2209–2210.
[87] M.S. Bernatowicz, Y.L. Wu, G.R. Matsueda, Urethane protected derivatives of 1-guanylpyrazole for the mild and efficient preparation of guanidines, Tetrahedron Lett. 34 (1993) 3389–3392.
[88] Y.R. Kim, S.E. Lee, C.M. Kim, S.Y. Kim, E.K. Shin, D.H. Shin, S.S. Chung, H.E. Choy, A. Progulske-Fox, J.D. Hillman, M. Handfield, J.H. Rhee, Characterization and pathogenic significance of *Vibrio vulnificus* antigens preferentially expressed in septicemic patients, Infect. Immun. 71 (2003) 5461–5471.